

## Article

# Synthesis of carbon-13 labelled carbonaceous deposits and their evaluation for potential use as surrogates to better understand the behaviour of the carbon-14-containing deposit present in irradiated PGA graphite

Payne, L, Walker, S., Bond, G., Eccles, Harry, Heard, P.J., Scott, T.B. and Williams, S.J.

Available at <http://clock.uclan.ac.uk/13924/>

*Payne, L, Walker, S., Bond, G., Eccles, Harry ORCID: 0000-0002-1652-3370, Heard, P.J., Scott, T.B. and Williams, S.J. (2016) Synthesis of carbon-13 labelled carbonaceous deposits and their evaluation for potential use as surrogates to better understand the behaviour of the carbon-14-containing deposit present in irradiated PGA graphite. Journal of Nuclear Materials, 470 . pp. 268-277. ISSN 0022-3115*

It is advisable to refer to the publisher's version if you intend to cite from the work.

<http://dx.doi.org/10.1016/j.jnucmat.2015.12.021>

For more information about UCLan's research in this area go to <http://www.uclan.ac.uk/researchgroups/> and search for <name of research Group>.

For information about Research generally at UCLan please go to <http://www.uclan.ac.uk/research/>

All outputs in CLoK are protected by Intellectual Property Rights law, including Copyright law. Copyright, IPR and Moral Rights for the works on this site are retained by the individual authors and/or other copyright owners. Terms and conditions for use of this material are defined in the [policies](#) page.



University of  
Central Lancashire  
UCLan

**CLoK**

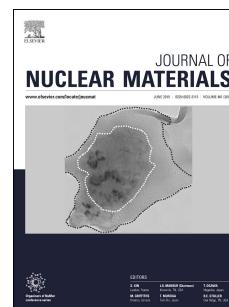
Central Lancashire online Knowledge  
[www.clok.uclan.ac.uk](http://www.clok.uclan.ac.uk)



# Accepted Manuscript

Synthesis of carbon-13 labelled carbonaceous deposits and their evaluation for potential use as surrogates to better understand the behaviour of the carbon-14-containing deposit present in irradiated PGA graphite

L. Payne, S. Walker, G. Bond, H. Eccles, P.J. Heard, T.B. Scott, S.J. Williams



PII: S0022-3115(15)30390-1

DOI: [10.1016/j.jnucmat.2015.12.021](https://doi.org/10.1016/j.jnucmat.2015.12.021)

Reference: NUMA 49514

To appear in: *Journal of Nuclear Materials*

Received Date: 6 April 2015

Revised Date: 15 December 2015

Accepted Date: 18 December 2015

Please cite this article as: L. Payne, S. Walker, G. Bond, H. Eccles, P.J. Heard, T.B. Scott, S.J. Williams, Synthesis of carbon-13 labelled carbonaceous deposits and their evaluation for potential use as surrogates to better understand the behaviour of the carbon-14-containing deposit present in irradiated PGA graphite, *Journal of Nuclear Materials* (2016), doi: 10.1016/j.jnucmat.2015.12.021.

This is a PDF file of an unedited manuscript that has been accepted for publication. As a service to our customers we are providing this early version of the manuscript. The manuscript will undergo copyediting, typesetting, and review of the resulting proof before it is published in its final form. Please note that during the production process errors may be discovered which could affect the content, and all legal disclaimers that apply to the journal pertain.

**Synthesis of carbon-13 labelled carbonaceous deposits and their evaluation for potential use as surrogates to better understand the behaviour of the carbon-14-containing deposit present in irradiated PGA graphite.**

**L. Payne<sup>a\*</sup>, S. Walker<sup>b</sup>, G. Bond<sup>b</sup>, H. Eccles<sup>c</sup>, P. J. Heard<sup>a</sup>, T. B. Scott<sup>a</sup> and S. J. Williams<sup>d</sup>.**

a) Interface Analysis Centre, HH Wills Physics Laboratory, University of Bristol, BS8 1TL, UK.

b) Centre for Materials Science, University of Central Lancashire, PR1 2HE, UK.

c) John Tyndall Institute for Nuclear Research, School of Computing, Engineering and Physical Sciences, University of Central Lancashire, PR1 2HE, UK.

d) Radioactive Waste Management, B587, Curie Avenue, Harwell Oxford, Didcot, OX11 0RH, UK

**Abstract**

The present work has used microwave plasma chemical vapour deposition to generate suitable isotopically labelled carbonaceous deposits on the surface of Pile Grade A graphite for use as surrogates for studying the behaviour of the deposits observed on irradiated graphite extracted from UK Magnox reactors. These deposits have been shown elsewhere to contain an enhanced concentration of  $^{14}\text{C}$  compared to the bulk graphite. A combination of Raman spectroscopy, ion beam milling with scanning electron microscopy and secondary ion mass spectrometry were used to determine topography and internal morphology in the formed deposits. Direct comparison was made against deposits found on irradiated graphite samples trepanned from a Magnox reactor core and showed a good similarity in appearance. This work suggests that the microwave plasma chemical vapour deposition technique is of value in producing simulant carbon deposits, being of sufficiently representative morphology for use in non-radioactive surrogate studies of post-disposal behaviour of  $^{14}\text{C}$ -containing deposits on some irradiated Magnox reactor graphite.

---

\*Corresponding author. Tel.: +44 (0) 117 331 17683

Email address: liam.payne@bristol.ac.uk (L. Payne)



## 1. Introduction

The decommissioning of the UK's first generation of gas-cooled, graphite-moderated (Magnox) reactors will lead to approximately 45,000 m<sup>3</sup> of irradiated reactor core graphite, with a packaged volume of 59,000 m<sup>3</sup>, for geological disposal [1]. An important radionuclide in safety assessments for the disposal of radioactive waste in a geological disposal facility (GDF) is the long lived isotope <sup>14</sup>C (half-life 5730 years) [2]. With an approximate total <sup>14</sup>C activity of more than 7000 TBq arising from Magnox graphite cores and the additional volume of graphite waste arising from advanced gas-cooled reactors (AGR) [2], investigation of the behaviour of <sup>14</sup>C associated with such wastes after closure of a geological disposal facility is important. Whilst reactor graphite has been extensively studied from a physio-mechanical standpoint, related to core integrity, relatively little research effort has been placed on understanding the behaviour of the graphite and constituent <sup>14</sup>C in a geological disposal environment.

Recent research [3] providing post mortem analysis of irradiated graphite from two Magnox reactor cores highlighted the presence of a carbonaceous deposit on the exposed surfaces of the graphite bricks (channel and interstitial walls) from one of the reactors that has a pronounced and markedly different morphology to the bulk graphite. The extent of this deposit is likely to be a worst case scenario and it is anticipated that not all Magnox reactors may contain such significant deposits. However, these surface deposits have been determined to have a significant <sup>14</sup>C content compared to the bulk graphite [4] that has been created via formation pathways discussed elsewhere [5]. It is not understood how these deposits will behave in a GDF setting in comparison to the graphite which it coats. Specifically there is a gap in the understanding of the release rate and magnitude of the labile <sup>14</sup>C fraction, of which <sup>14</sup>C located in deposited material may contribute significantly, with this labile fraction expected to achieve relatively early release in the lifetime of a GDF [6]. The pronounced "cauliflower-like" morphology observed is not unique to nuclear reactors and similar morphologies have been commonly reported within the scientific literature for carbon from a range of deposition techniques unrelated to nuclear applications [7-11]. At present such deposits are of specific interest in geological disposal of graphite waste from the decommissioning of Magnox reactors, as the deposited material may be present and represent a significant fraction of the labile <sup>14</sup>C.

The Magnox reactors represent the first generation of gas-cooled reactors in the UK that used carbon dioxide (CO<sub>2</sub>) as the primary coolant and a honeycomb network of graphite bricks to

provide neutron moderation. During reactor operation significant amounts of carbon monoxide (CO) was produced from the CO<sub>2</sub> coolant. This CO in turn can be radiolytically polymerised to form a carbonaceous deposit on free surfaces [12]. This non-graphitic carbon deposit is significantly more chemically reactive to air than the underlying graphite [12, 13]. During the lifetime of some Magnox reactors, small quantities of methane gas were injected into the coolant gas to inhibit weight loss of the graphite core due to radiolytic oxidation [14]. Methane (CH<sub>4</sub>) is a precursor for carbonaceous deposits that form a sacrificial layer protecting the underlying graphite from excessive weight loss [15] and reduction in mechanical strength [16]. It is assumed nitrogen incorporation during deposit formation is the subsequent production route for the high <sup>14</sup>C levels observed.

CH<sub>4</sub> is also a commonly utilised feedstock gas for the production of diamond and other carbon coatings by the process of chemical vapour deposition (CVD) [17]. The growth of carbon materials by CVD involves the excitation of a carbon-containing precursor gas using a thermal or plasma energy source that creates activated radicals that will bond to a suitable exposed surface. Therefore, even though differences exist in the formation of carbonaceous deposits from CO and CH<sub>4</sub>, both include the activation of carbon-containing gas creating activated carbon species that will bond to surfaces. Recent work [3] showed that graphite from the Oldbury Magnox power station, which had methane introduced into the coolant gas, had a significant deposit on the fuel and interstitial channel walls of the graphite bricks. This suggested that the deposit formed may be due to methane. A comparison of the morphology and density of such deposits will help determine whether a <sup>13</sup>C methane deposit can be used as a simulant for the surface deposit found on irradiated graphite in further work. If <sup>13</sup>C carbonaceous deposits can be used as a simulant for the deposits seen on irradiated graphite it will allow easier, non-radioactive investigations of the potential release of <sup>14</sup>C from deposits on irradiated graphite in a geological disposal environment including the potential microbial interaction with such material. If the deposits observed on the graphite behave differently to the underlying graphite it may lead to a significantly different release rate for <sup>14</sup>C from the deposit than from the underlying graphite when contacted by groundwater some time after the closure of a geological disposal facility. Microbial colonisation may also be more likely on the deposit than the underlying graphite due to the increased surface area due to the amorphous nature of the material.

The use of a <sup>13</sup>C simulant allows wider access into the research of nuclear graphite, which contains many other radionuclides such as <sup>60</sup>Co, as facilities to handle radioactive materials are not required. Isotopic differences in the precursor material should not alter the chemical

nature and/or effect the chemistry of the deposited carbon material. To this end,  $^{13}\text{C}$  has previously been used as a common isotopic tracer in biological systems [18] and implanted in graphite [19] as a non-radioactive proxy for  $^{14}\text{C}$ . In the current work we demonstrate the use of microwave plasma CVD to create a carbonaceous layer on graphite substrates that exhibit similar morphologies and densities to deposits observed to have formed in-service on Magnox graphite moderator blocks. The non-radioactive isotope  $^{13}\text{C}$  was selected as a tracer during CVD deposition such that deposit-substrate interfaces could be clearly resolved using imaging mass spectrometry analysis to determine the degree of material mixing and substrate etching.

The present work is part of a larger programme (C14-BIG) directed at gaining a better understanding and predicting the release of graphite derived  $^{14}\text{C}$  from a GDF and the influence of microbial activity under alkaline conditions expected to predominate for a significant time in a cement-based near field of a geological disposal facility after closure.

## 2. Experimental

### 2.1. Sample preparation

Pile Grade A (PGA) graphite was provided by Magnox Limited as a surplus material from the commissioning of the Wylfa nuclear power reactors, Wales. This graphite was trepanned into cores of 12 mm diameter using a stainless steel coring tool. The cores were then cut into 2 mm thick discs using a South Bay Technology Inc. Model 650 low speed diamond cutting wheel with deionised water used as coolant. This process gave a flat surface that was a

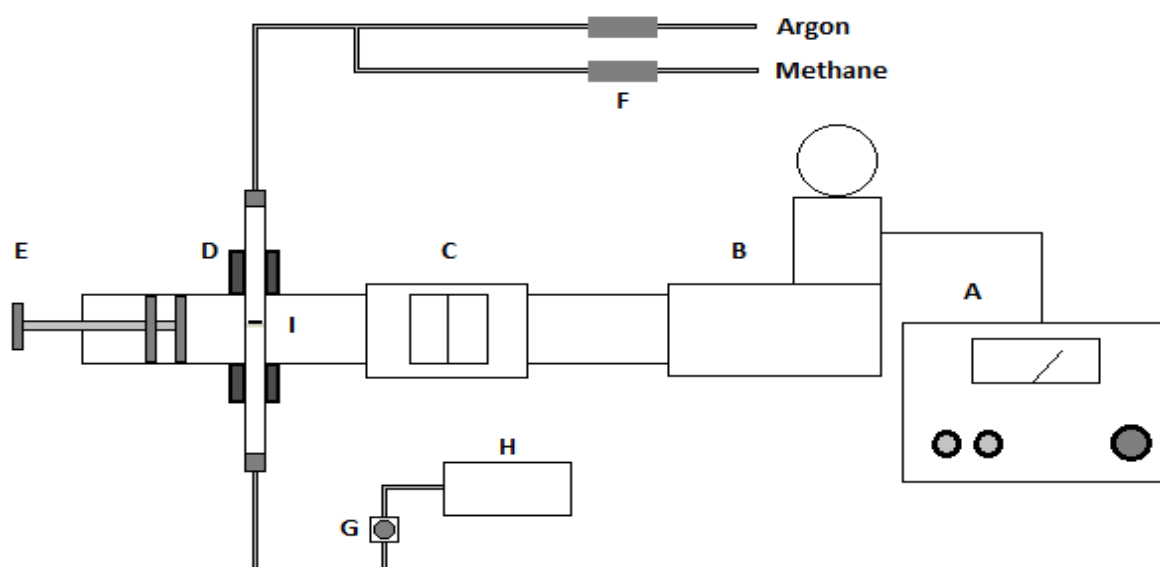


Figure 1, Schematic diagram of a single mode microwave plasma chemical vapour deposition (MPCVD) system. (A: variable power microwave controller (max. 1000 W); B: air-cooled microwave generator; C: water-cooled circulator; D: 4 port single mode TE01 microwave cavity; E: double plunge microwave tuner; F: mass-flow controllers; G: diaphragm vacuum pump; H: mass spectrometer; I: quartz tube containing a graphite disc on a porous glass sinter.)

suitable substrate for deposition. Subsequently  $^{12}\text{C}$  and  $^{13}\text{C}$  carbonaceous deposits were formed on the graphite surfaces using microwave plasma chemical vapour deposition (MPCVD), Figure 1.

Coating was carried out using a computer-controlled 2.45 GHz microwave generator (variable power output – maximum 1000 Watts),  $\text{TE}_{01}$  single mode cavity (Sairem downstream plasma source WR340), double plunge microwave tuner, mass-flow controllers (MFC) and a carrier (Argon) and precursor gas at a total flow rate of  $50\text{ cm}^3\text{ min}^{-1}$ . Sample coatings were made at methane concentrations of 2, 10 and 20% for  $^{12}\text{CH}_4$  and 2% for  $^{13}\text{CH}_4$ . For coating, each cylindrical PGA graphite disc was placed on a glass sinter situated inside a quartz tube which was aligned to position the disc within the centre of the waveguide. The tube was then connected to the mass-flow controllers, a gas flow was established and then the system was placed under a low vacuum. Once a 1000 Pa system pressure had been achieved the microwave generator was switched on and the microwave reflectance was reduced, as much as possible, using the double plunge microwave tuner. Once the microwave reflectance was tuned the CVD coating process was left to proceed for a period of 30 minutes [20]. Additionally, deposition was performed at varying pressures (1000, 5000, 10 000 Pa), however a flow rate of  $50\text{ cm}^3\text{ min}^{-1}$  for the gas mixture did not achieve a system pressure of less than 700 Pa. A lower flow rate of  $20\text{ cm}^3\text{ min}^{-1}$  was applied at 10%  $^{12}\text{CH}_4$  so that a system pressure of 500 Pa could be achieved, additionally growth was performed at 10 Pa system pressure at this reduced flow rate.

1-2 mm particles were also produced alongside the disc samples due to crucible size restrictions for the Linkam catalyst stage for Raman spectroscopy. Additional PGA graphite was provided by the National Nuclear Laboratory (NNL). This graphite was sectioned into smaller rectangular sheets using a JCB toolbox saw and then cut into smaller monoliths using an Erbauer ERB180C tile cutter (with no coolant) thus making the graphite more manageable. The graphite monoliths were then put into a metal container and placed into a 10-ton hydraulic press, where a pressure between 5-10 tonnes of pressure was used to break the graphite down into smaller pieces. The pieces were then subsequently filtered using a 3 compartment Fisherbrand stainless steel sieve (aperture sizes:  $>2\text{ mm}$ ,  $1\text{-}2\text{ mm}$  and  $<1\text{ mm}$ ) and the 1-2 mm particles were retained for subsequent microwave deposition. Both the larger and smaller pieces were repeatedly pressed until all of the graphite was left as a mixture of either particles or powder, following sieving.

A selection of virgin PGA samples (i.e. without deposit) and irradiated graphite specimens extracted by trepanning from a Magnox power station were also analysed for comparison, exact details previously described in [4].

## *2.2. Scanning electron microscopy/ Focused ion beam*

A Helios NanoLab 600i combined SEM/FIB system (FEI, Oregon USA) was used to obtain scanning electron micrographs. The focused ion beam (FIB) was utilised to precision mill trenches to allow the thickness and morphology of the deposit to be determined with nanometre accuracy and to allow subsequent analysis using other techniques. Electron micrographs were acquired using an accelerating voltage of 15 kV, an electron beam current of 0.17 nA and a dwell time of 100  $\mu$ s. Trenches were FIB milled with the use of a  $\text{Ga}^+$  ion source with an accelerating voltage of 30 kV. A Selective Carbon Mill (SCM) gas was used throughout to enhance milling rates. The SCM admits small amounts of water vapour directly over the milling area, promoting gasification of the milled material, enhancing the etch rate and reducing redeposition. It also minimises beam damage and therefore reduces the need to deposit platinum on the surface as a protective measure. Initially a 20 nA beam current was used to generate coarsely defined trenches, with subsequent incremental reductions in ion current to reach a final beam current of 0.9 nA for surface finishing. The milled trenches had approximate dimensions of 50  $\mu$ m x 56  $\mu$ m x 20  $\mu$ m (x, y and z respectively). The trench faces were smooth and flat, allowing for direct and high spatial resolution observation of structures and features.

## *2.3. Magnetic Sector-Secondary Ion Mass Spectrometry*

For isotopic analysis of the samples, an in-house built magnetic sector secondary ion mass spectrometer (MS-SIMS) was utilised. Full details of the system are described elsewhere [21]. In summary the system comprised of a focused gallium ion gun (FEI electronically variable aperture type) fitted to a Vacuum Generators model 7035 double-focusing magnetic sector mass analyser with a channeltron detector. The sample was held at a 4 kV potential during analysis. The equipment was controlled using PISCES software, written in-house by Dayta Systems Ltd (Thornbury, UK). The system was capable of providing selected ion mapping and depth profiling with sub-micron resolution. MS-SIMS analyses were performed in negative ion mode for both spectral acquisition and secondary ion imaging. Mass spectra and depth profiles were initially acquired from 4

different areas of the 2%  $^{12}\text{C}$  and  $^{13}\text{C}$  methane deposits, detecting mass/charge ( $m/z$ ) signals at 12, 13, 24 and 26 Da. These ion signals are generated due to the  $\text{C}^-$  and  $\text{C}_2^-$  ions derived from sputtered  $^{12}\text{C}$  and  $^{13}\text{C}$  respectively. Mass spectra were obtained by scanning through the mass range 0-100 Da in 0.05 Da steps, with duration of 100 ms per step and 200 s in total. Data acquisition was performed at a low magnification to reduce beam damage (area analysed  $\sim 0.25 \text{ mm}^2$ ) and with a 3 nA beam current. Identification and calibration of the exact  $m/z$  values for use in subsequent depth profiles and images were achieved with the use of these survey spectra.

Depth profiles record the ion yield intensity from selected sputtered analyte ions over time while rastering the ion beam over a selected area. As the deposits are suitably thick it is not anticipated that the depth profile will sputter enough material to immediately expose the underlying graphite. This allows the signal to be averaged over a set period of time and then the ratio between signals to be compared. Depth profiles were acquired for 1800 s with a beam current of 3 nA and area analysed of approximately  $2500 \mu\text{m}^2$ . Electronic gating was used throughout to eliminate signal created at the margins of the etched area. Signal averages and ratios were calculated from 200 s to 1800 s, disregarding the first 200 s of data as this was the observed transient period for the experiment.

The species compared were the  $\text{C}_2^-$  ions at 24 and 26 Da, rather than 12 and 13 Da, due to the strong signals obtained from these species, and also to avoid some prominent mass interferences. Interference peaks are difficult to eliminate, however the use of the  $\text{C}_2^-$  peak is appropriate as the present work is not trying to identify trace elements but aiming to investigate whether the surface deposits are formed of  $^{13}\text{C}$ , to what extent  $^{13}\text{C}$  is incorporated into the graphite and how thick the overall deposit is.

Secondary ion images were recorded from the FIB milled trenches using the  $\text{C}_2^-$  ions (24 and 26 Da). The images were obtained by selecting the  $m/z$  ratio of the ion of interest, and then raster scanning the ion beam over a defined area of the sample. The images presented in this paper were acquired over a total area of approximately  $0.0225 \text{ mm}^2$ . Each image was acquired over a 60 second period using a 0.3 nA beam current to give the best possible spatial resolution whilst still maintaining sufficient ion signal.

#### *2.4. Catalyst stage Raman spectroscopy*

A CCR1000 catalyst stage reactor system connected to a T95 system controller and LinkPad interface (Linkam, Surrey UK) was used for the thermal oxidation of the PGA graphite 1-2



mm particles. For *in situ* spectral acquisition, a LabRAM HR800 confocal Raman microscope (Horiba Jobin Yvon, Kyoto Japan) was used. The sample was heated up in the crucible inside of the catalyst stage from room temperature up to 600 °C (at 10 °C min<sup>-1</sup>), with a 50 cm<sup>3</sup> min<sup>-1</sup> flow of air. Spectra were acquired using a 532 nm laser, a 50X long-working distance objective, a 300 g mm<sup>-1</sup> grating, and spectral acquisition times of 25 s every 50 °C. The heating regime and the spectral acquisition parameters for automated analysis were controlled using a built-in Linkam module script in the Horiba LabSpec 6 software package. The Raman spectroscopy system was calibrated using the 520 cm<sup>-1</sup> peak from a silicon crystal. Spectral analysis, during thermal oxidation in air, of virgin PGA graphite and PGA graphite with <sup>12</sup>C and <sup>13</sup>C carbonaceous deposits was carried out to analyse the thermal profile of the surface material (i.e. graphite substrate) and the “cauliflower-like” carbonaceous deposit. This technique allows for analysis of the thermal oxidation properties/reactivity of the different carbon materials and also surface chemical changes due to thermal oxidation.

### 3. Results

#### 3.1. Scanning Electron Microscopy

The deposit formed on irradiated graphite taken from Oldbury Magnox reactor has a distinct and pronounced morphology, Figure 2a, compared to virgin PGA graphite, Figure 2b [3]. For comparison, electron micrographs of the 2% <sup>12</sup>CH<sub>4</sub> and 2% <sup>13</sup>CH<sub>4</sub> deposits can be seen in Figure 3, a and b respectively. The distinction between deposit and underlying graphite should be noticeable due to the lack of characteristic features in the deposit that are routinely seen in all PGA graphite such as shrinkage cracks and ligaments between pores [22], Figure 4. The deposits found on irradiated graphite have a ‘cauliflower-like’ appearance due to an agglomeration of irregular spheres, Figure 5. After FIB milling the internal morphology of the 2% <sup>13</sup>CH<sub>4</sub> and 2%, 10% and 20% <sup>12</sup>CH<sub>4</sub> deposited samples can be seen in Figure 6a, b, c, and d respectively.

The 2% <sup>12</sup>C and <sup>13</sup>C methane CVD deposits were observed to have a porous, ‘feathery’ texture that appears to be significantly less dense than the underlying graphite. For the irradiated graphite however, there was very little distinction in density or fine structure between the deposit and the underlying graphite (the deposit appears to have a lower porosity compared to virgin PGA, Figure 5). It is possible that the underlying PGA graphite in the

246 irradiated samples is protected from radiolytic oxidation by the carbon deposit, leading to the  
247 deposit and underlying graphite being difficult to distinguish [15].

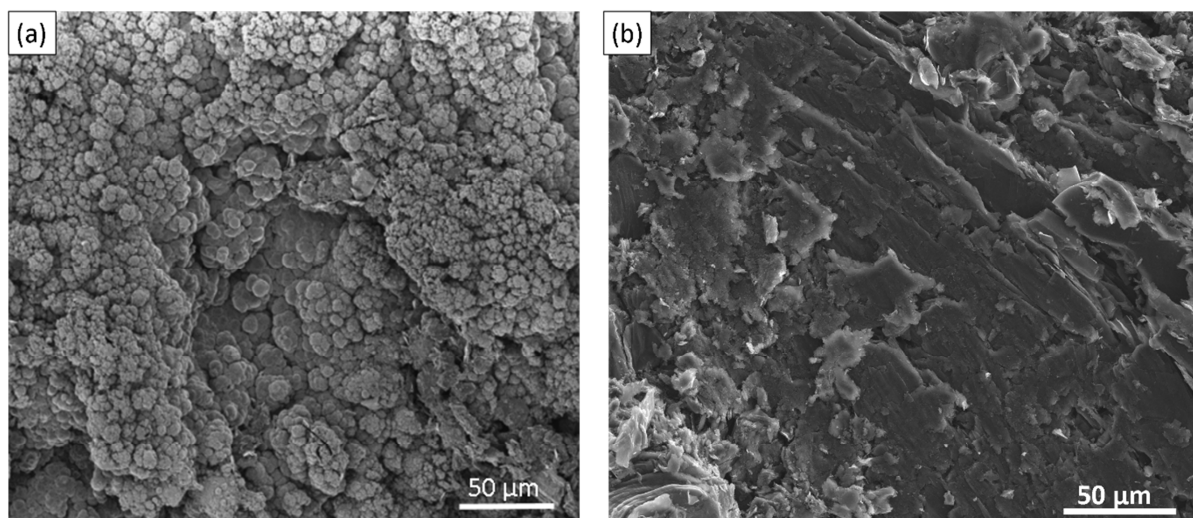


Figure 2, a) Focused ion beam image of deposit found on irradiated graphite surface, from [4] and b) virgin PGA surface.

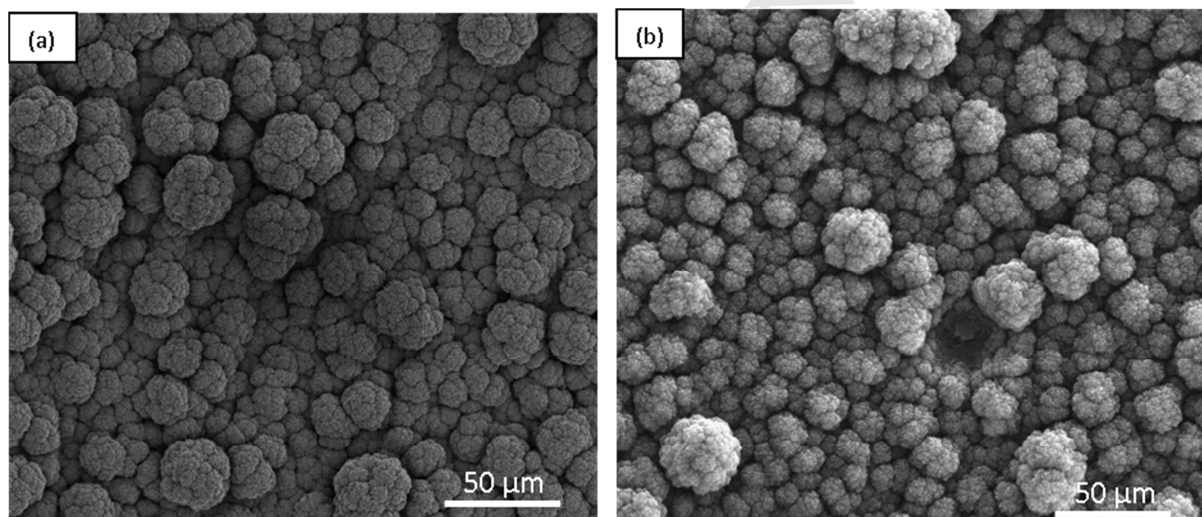


Figure 3, Scanning electron micrographs from  $^{12}\text{C}$  (a) and  $^{13}\text{C}$  (b) carbonaceous deposits on Pile Grade A graphite, system pressure 1000 Pa.

248  
249 Further investigation using greater methane concentrations showed increases in the apparent  
250 density of the deposit (which was only determined visually), Figures 6 (b), (c) and (d), that  
251 are more closely comparable to the deposit found on irradiated graphite. Deposits produced at  
252 system pressures of 5000 and 10000 Pa were of different morphology, instead comprising an  
253 agglomeration of spherical deposits that were not as extensive or as thick as those grown at  
254 the lower pressure of 1000 Pa. Reducing the flow rate to  $20 \text{ cm}^3 \text{ min}^{-1}$  allowed a system  
255 pressure of 500 Pa to be achieved, however even though the surface topography of the



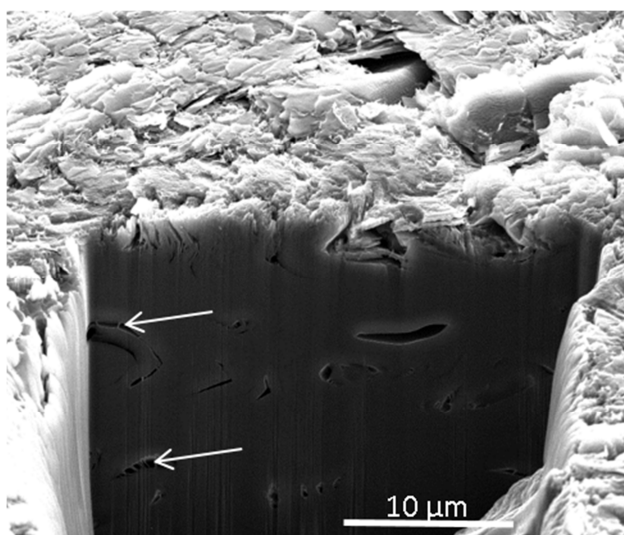


Figure 4, Scanning electron micrograph from cross section of an uncoated Pile Grade A graphite after FIB milling showing characteristic cracking and ligaments, shown with the arrows.

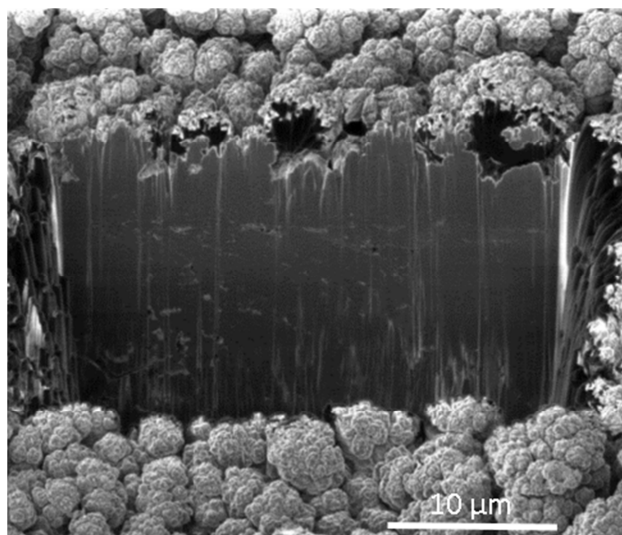


Figure 5, Focused ion beam image from cross section of channel wall trepanned sample from a Magnox reactor [3].

deposit was similar to irradiated material and the other cauliflower-like deposits formed, the internal morphology exhibited extensive porosity and this did not appear suitable as a simulant, Figure 7(a). Conversely, growth at a system pressure of 1000 Pa at this reduced flow rate formed a deposit that was very similar to that grown at  $50 \text{ cm}^3 \text{ min}^{-1}$ , Figure 7(b). The deposit formed at 1000 Pa pressure at 10% methane concentration showed the closest resemblance to those seen on Oldbury irradiated Magnox graphite and was deemed to be the most suitable for use as a simulant.

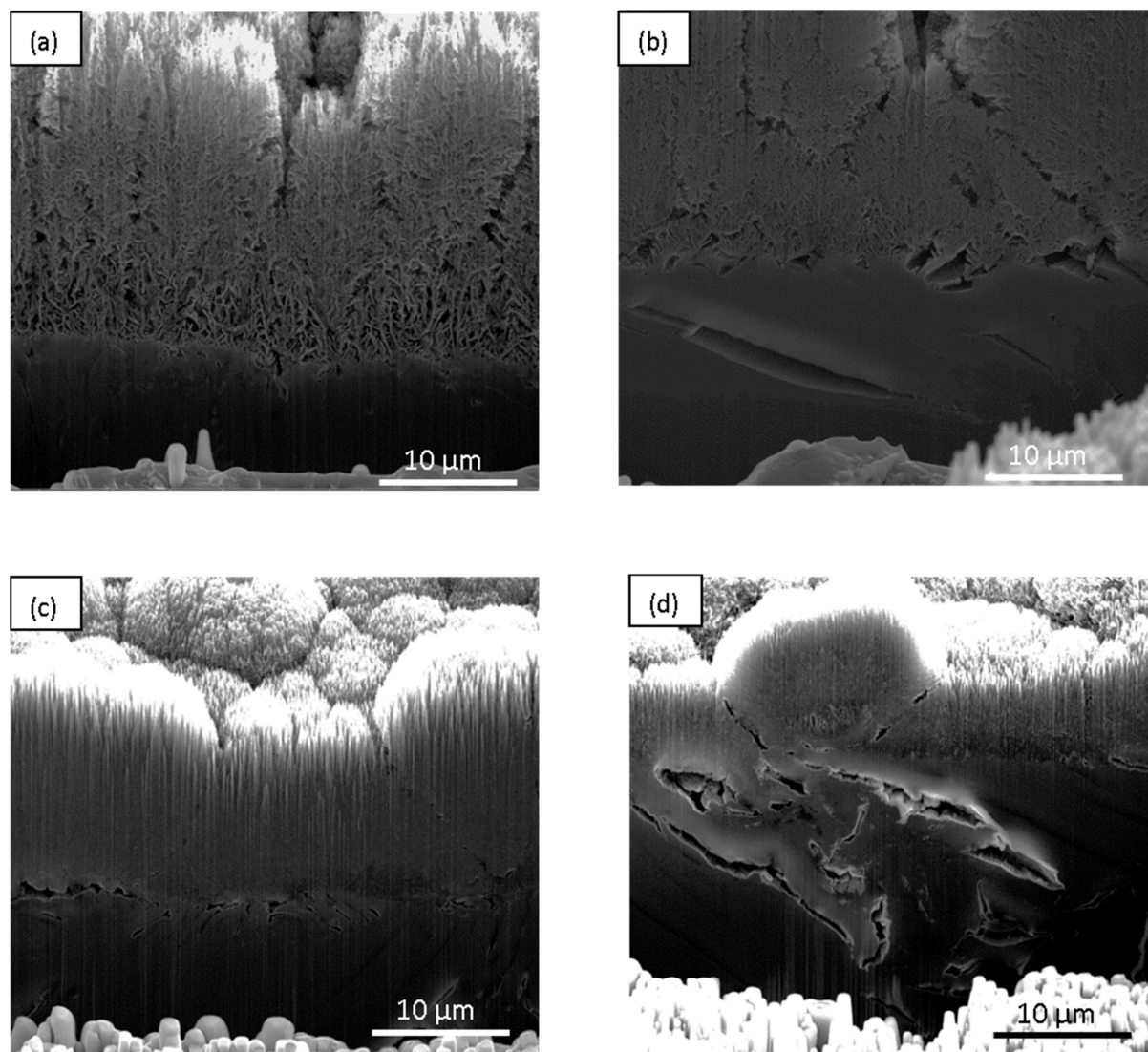


Figure 6. Scanning electron micrographs showing the ion beam milled cross sections for 2%  $^{13}\text{CH}_4$  (a) and 2% (b), 10% (c) and 20% (d)  $^{12}\text{CH}_4$  deposited samples, all at system pressure of 1000 Pa.

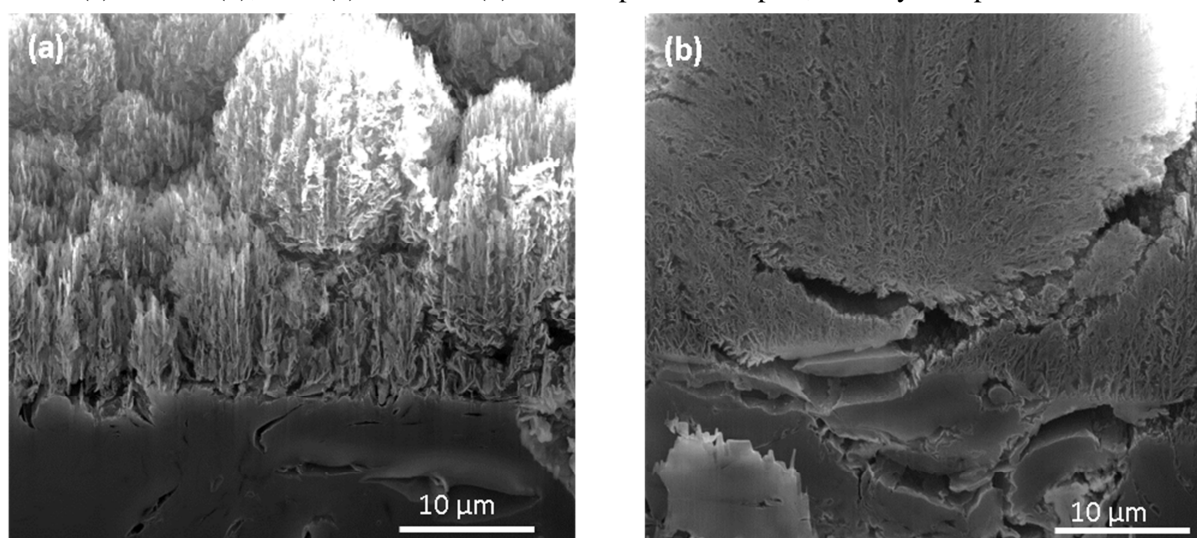


Figure 7. Scanning electron micrographs showing the ion beam milled cross sections at system pressures of 500 (a) and 1000 (b) Pa, flow rate  $20 \text{ cm}^3 \text{ min}^{-1}$ .

### 272 3.2. Secondary Ion Mass Spectrometry

273 Survey spectra from the 2% methane  $^{12}\text{C}$  and  $^{13}\text{C}$  deposits are shown in Figures 8 (a) and (b)  
 274 respectively. Signals recorded at mass/charge peaks of 13 Da ( $^{13}\text{C}^-$  and 26 Da ( $^{13}\text{C}_2^-$ )) are  
 275 significantly greater in the  $^{13}\text{C}$  deposit compared to the  $^{12}\text{C}$  deposit, although these signals are  
 276 also present in the  $^{12}\text{C}$  sample due to  $^{12}\text{CH}^-$  and  $^{12}\text{CN}^-$  species respectively. The mean ratio  
 277 ( $n=4$ ) between the peak heights at 26 Da and 24 Da for the  $^{12}\text{C}$  deposit was found to be  $0.14 \pm$   
 278  $0.03$ . The mean ratio ( $n=4$ ) for the  $^{13}\text{C}$  deposit was  $115.3 \pm 19.1$ . This increase of several  
 279 orders of magnitude is strong evidence that the deposit is predominately  $^{13}\text{C}$  as the interfering  
 280 peak from  $^{12}\text{CH}$  at 13 Da is unlikely to be higher in the  $^{13}\text{C}$  sample. The errors given here are  
 281 likely to be due to the strong dependence of signal intensity on location and geometry of the  
 282 sample in the SIMS system [23].

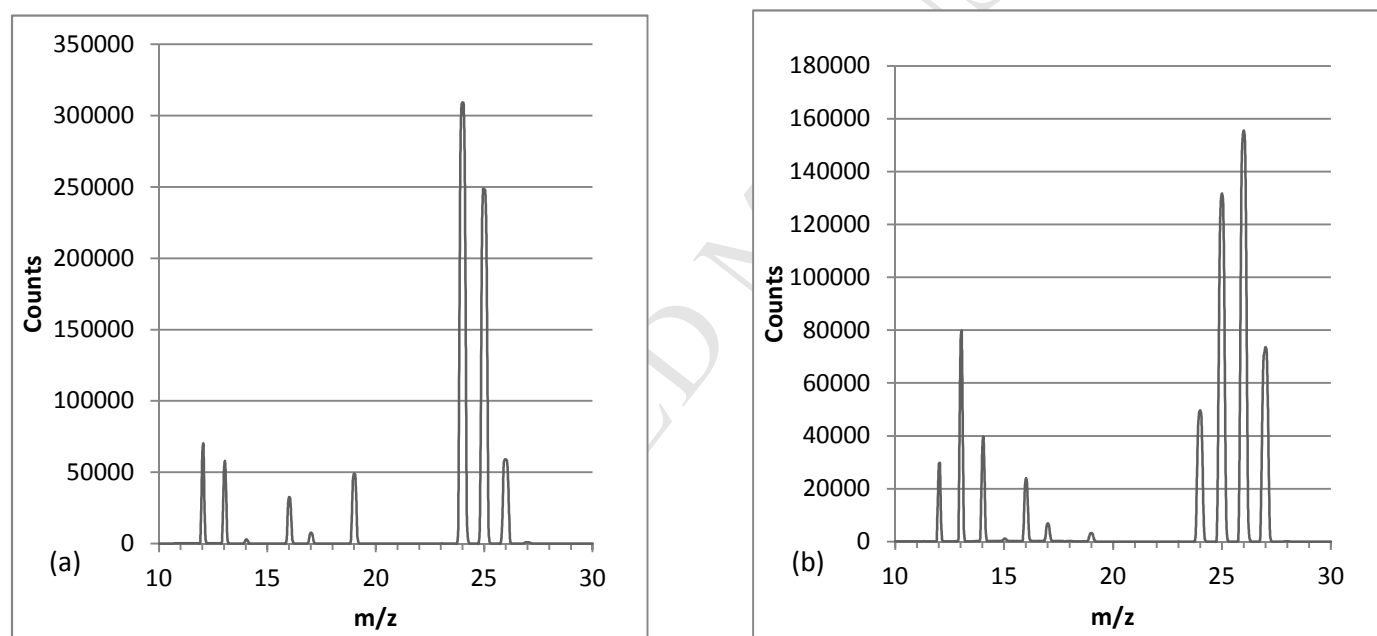


Figure 8, SIMS spectra from 2% methane  $^{12}\text{C}$  (a) and  $^{13}\text{C}$  (b) deposit.



283 The areas analysed were selected randomly and the only criteria for examination was that  
 284 they produced sufficient SIMS signal to allow analysis. Due to the surface not having a  
 285 uniform, flat surface there are likely to be topographic effects that will affect the signal  
 286 recorded. This has been studied by other authors [23-25] with suggestions that the changes  
 287 may be due to the incident angle of the beam, the height of the features and variations in the  
 288 electric field due to topographic features that may lead to trajectory changes of the secondary  
 289 ions [24].

290 SIMS ion signal maps have been recorded for 26 Da and 24 Da for a  $^{13}\text{C}$  sample, Figure 9 (a)  
 291 and Figure 9 (b) respectively. For the  $^{13}\text{C}$  deposit the mass peak signal at 26 Da is present  
 292 primarily on the deposit with a significant reduction in signal in the underlying graphite with  
 293 the 24 Da signal being the reverse, with a more intense signal recorded in the underlying  
 294 graphite than in the deposit. This shows that the  $^{13}\text{C}$  is deposited on top of the underlying  
 295 graphite. The signal at the bottom of the trench has a relatively high intensity for both 24 and  
 296 26 Da, and this may be due to re-deposition of sputtered material originating from the  $^{13}\text{C}$   
 297 deposit during FIB milling of samples [26].

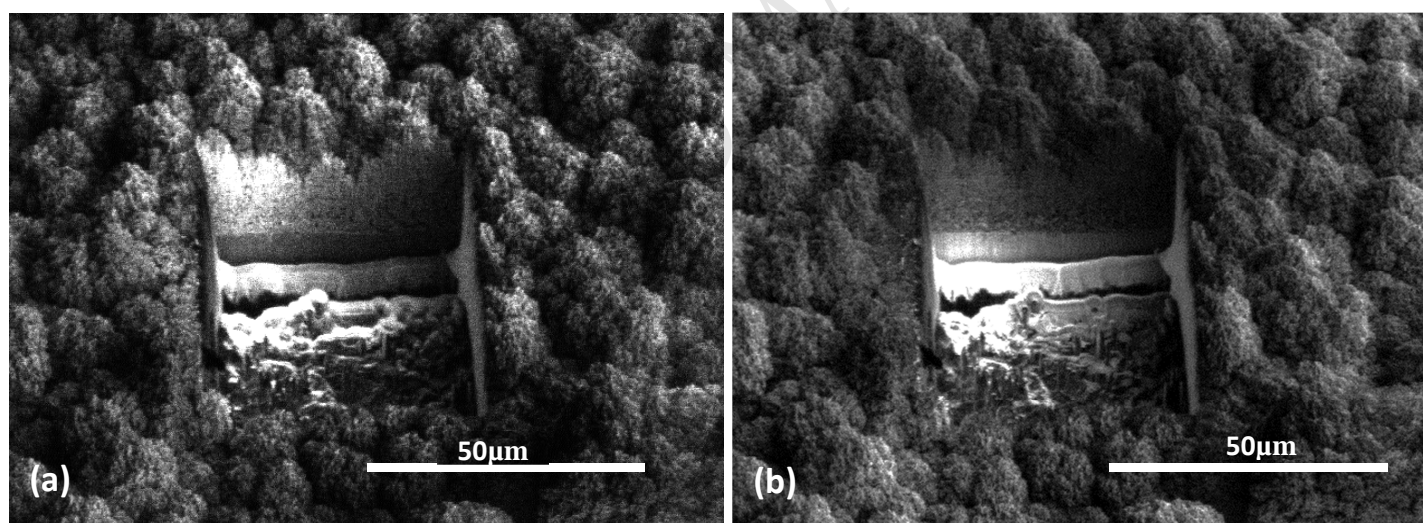


Figure 9, Secondary Ion signal maps for 26 Da (a) and 24 Da (b) from cross section of  $^{13}\text{C}$  carbonaceous deposit on top of Pile Grade A graphite after FIB milling.

### 3.3. Catalyst stage Raman spectroscopy

299 A three-vectored graph displaying Raman shift, intensity and temperature (x, y and z axis  
 300 respectively) was used to illustrate the Raman spectra at each temperature during the thermal  
 301 oxidation experiment. The Raman spectra are displayed between  $1100 - 1700 \text{ cm}^{-1}$  to allow  
 302 the critical peaks related to both  $^{12}\text{C}$  and  $^{13}\text{C}$  carbonaceous materials to be compared. The  $^{12}\text{C}$

303 peaks are the  $^{12}\text{D}$  peak at  $\sim 1350\text{ cm}^{-1}$  and the  $^{12}\text{G}$  peak at  $\sim 1575\text{ cm}^{-1}$  and the  $^{13}\text{C}$  peaks are  
 304 the  $^{13}\text{D}$  peak at  $\sim 1300\text{ cm}^{-1}$  and the  $^{13}\text{G}$  peak at  $\sim 1525\text{ cm}^{-1}$ .

### 305 3.3.1. Virgin PGA

306 The thermal oxidation spectral profile for a virgin PGA graphite 1-2 mm particle is shown in  
 307 Figure 10. This spectral profile shows that there was a negligible change in the intensity of  
 308 the D and G peaks between  $50 - 600\text{ }^{\circ}\text{C}$ . This indicates that between  $50 - 600\text{ }^{\circ}\text{C}$  the surface  
 309 of the PGA graphite undergoes very minimal surface oxidation and that the PGA is mostly  
 310 unreactive.

311 As the surface of the virgin PGA material remains relatively unchanged during thermal  
 312 oxidation it will readily allow for any spectral changes, due to the thermal oxidation of  $^{12}\text{C}$   
 313 and  $^{13}\text{C}$  carbonaceous deposits, to be isolated.

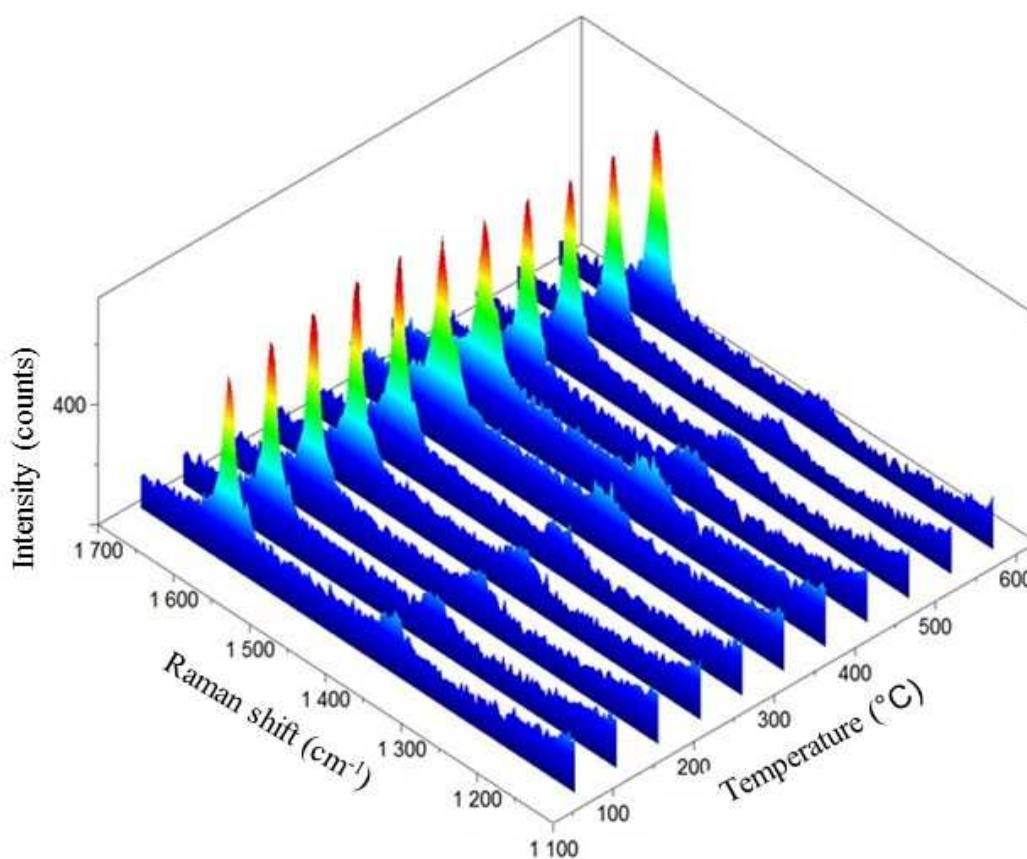


Figure 10, *In situ* Raman spectral analysis, during thermal oxidation, of a 1-2 mm virgin PGA graphite particle.

314

3.3.2. PGA Graphite with  $^{12}\text{C}$  and  $^{13}\text{C}$  Deposits

The thermal oxidation spectral profiles for a 2 %  $^{12}\text{CH}_4$  and  $^{13}\text{CH}_4$  deposit on a PGA graphite particle are shown in Figures 11 and 12 respectively. Figure 11 shows that there is a noticeable decrease in the  $^{12}\text{D}$  peak intensity between 400 – 600 °C. This indicates that the  $^{12}\text{C}$  carbonaceous deposit begins to thermally oxidise at approximately 400 °C and appears to have been completely removed by 600 °C indicated by the intensity of the  $^{12}\text{D}$  peak at 600 °C, showing the spectral profile of the virgin PGA graphite material.

There is a noticeable decrease in the  $^{13}\text{D}$  &  $^{13}\text{G}$  peak intensities between 450 – 600 °C in Figure 12, which are solely present due to the  $^{13}\text{C}$  carbonaceous deposit. This indicates that the  $^{13}\text{C}$  carbonaceous deposit begins to thermally oxidise at approximately 450 °C and appears to have been completely removed by 600 °C indicated by the absence of the  $^{13}\text{D}$  &

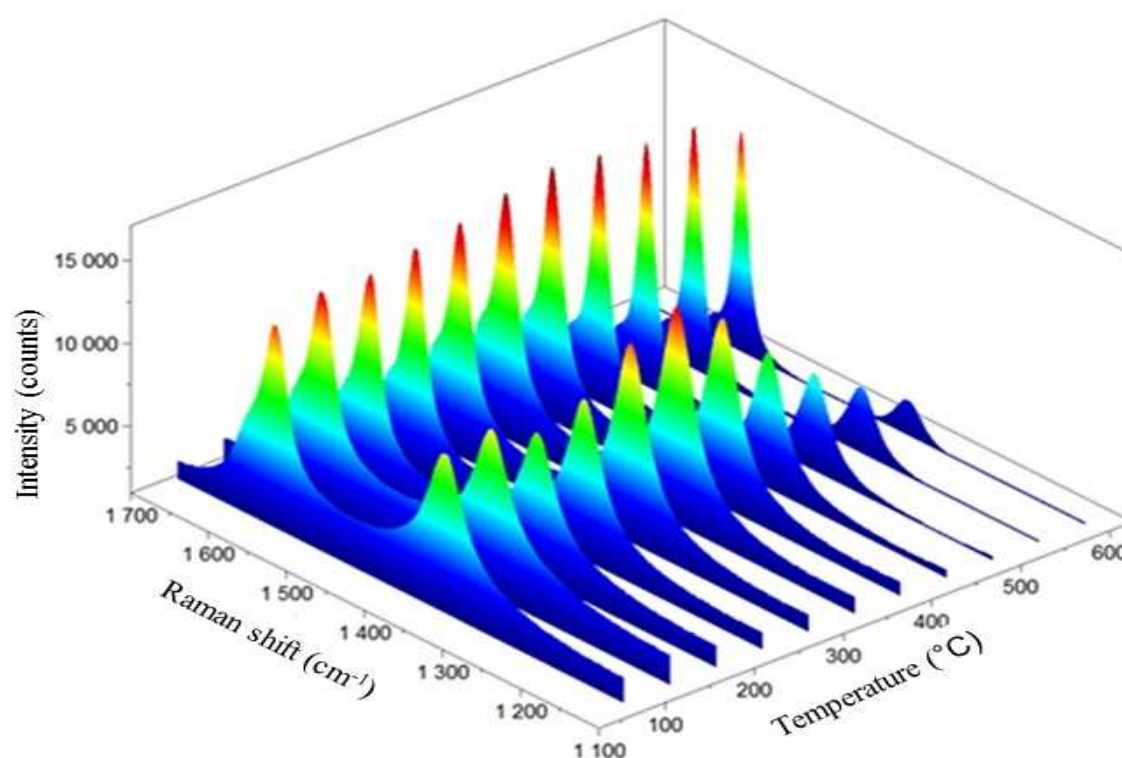


Figure 11, *In situ* Raman spectral analysis, during thermal oxidation, of a 2%  $\text{CH}_4$   $^{12}\text{C}$  carbonaceous deposit on a 1-2 mm PGA graphite particle

$^{13}\text{G}$  peaks at 600 °C, showing the spectral profile of the virgin PGA graphite material.

The intensities of the  $^{12}\text{D}$  and  $^{12}\text{G}$  peaks (PGA graphite) do not decrease but in fact increase relative to the decrease in the intensities of the  $^{13}\text{D}$  and  $^{13}\text{G}$  peaks ( $^{13}\text{C}$  carbonaceous

deposit), which also illustrates that the surface of the virgin PGA material, as a base substrate, remains relatively unchanged during thermal oxidation.

As the Raman peaks associated with the deposits decrease between 400 - 600 °C it indicates that the carbonaceous material on the surface has a similar oxidation temperature to that of the carbonaceous deposits found on irradiated PGA graphite (M. P. Metcalfe, personal communication, 11<sup>th</sup> November 2013).

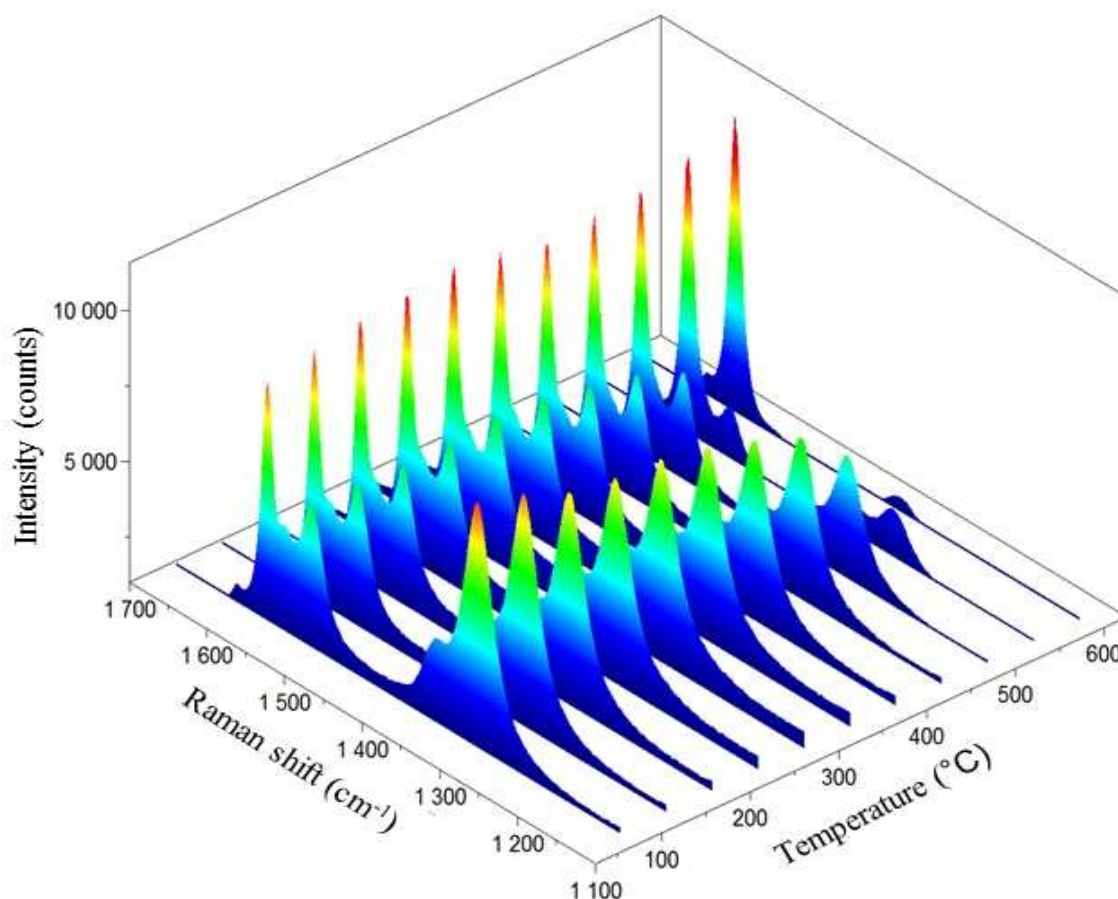


Figure 12, *In situ* Raman spectral analysis, during thermal oxidation, of a 2% CH<sub>4</sub> <sup>13</sup>C carbonaceous deposit on a 1-2 mm PGA graphite particle

Figure 13 illustrates the isothermal profiles of virgin PGA graphite, irradiated PGA graphite deposit & a <sup>12</sup>C microwave simulant deposit at 450 °C, in air, over a 50 hour period. The oxidation of virgin PGA graphite is negligible whereas the irradiated PGA graphite deposit & the C-12 microwave simulant deposit show significantly greater rates of oxidation and are clearly more reactive. Initially the rates of thermal oxidation remain fairly similar for the first 5 hours for the irradiated PGA graphite deposit & the <sup>12</sup>C microwave simulant deposit but for the next 45 hours the irradiated PGA graphite deposit shows a greater rate of thermal



oxidation. This deviation in rates of reactivity may be due to irradiated damage caused to the underlying PGA graphite in the irradiated PGA graphite sample whereas the underlying PGA graphite in the microwave simulant underwent no irradiation and started off as pristine virgin PGA graphite. However the microwave simulant carbonaceous deposit reactivity seen in the TGA isothermal data shows a similar reactivity to that of the carbonaceous deposit seen in irradiated PGA graphite.

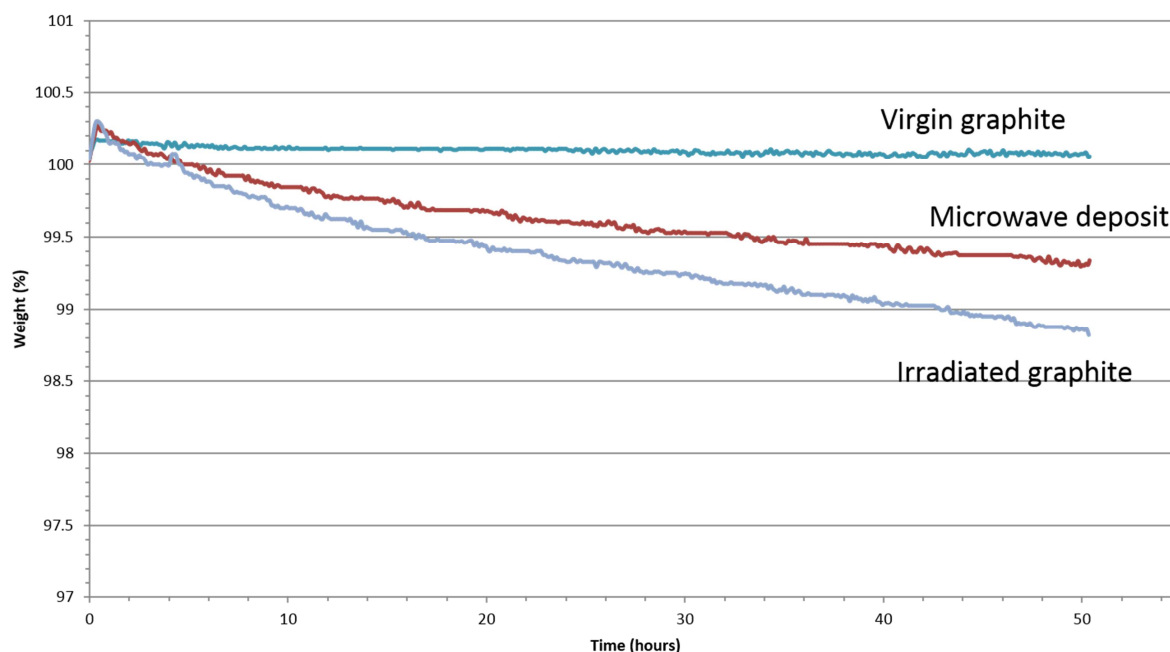


Figure 13, Thermograms from virgin PGA graphite, irradiated PGA graphite and  $^{12}\text{C}$  simulant deposit on PGA graphite examined at 450 °C, in air, over a 50 hour period.

#### 4. Discussion

Previous examination [3] of irradiated graphite from Magnox reactors has shown that during generation lifetime a carbonaceous deposit can be formed on the fuel and interstitial channel walls of the graphite moderator that has a markedly different morphology to the underlying PGA graphite. This work aimed to form a similar carbonaceous deposit using  $^{13}\text{C}$  precursor gas to allow subsequent investigation of the behaviour of such deposits in leaching and microbial studies pertinent to examining graphite degradation and  $^{14}\text{C}$  release in a GDF [27]. Use of a simulant allows future experiments to be performed more easily than using irradiated graphite due to a removal of the need to work with radioactive materials. However, the use of simulants necessitates care to ensure that they are representative of the properties being examined. With the use of several experimental techniques (FIB, SEM, MS-SIMS, Raman) this work has examined the internal morphology as well as the surface



topography of carbonaceous deposits formed using microwave plasma CVD and compared them to irradiated graphite trepanned from a Magnox power station graphite core. Microwave plasma CVD has been used to form adherent carbonaceous deposits on the surfaces of virgin (unirradiated) PGA graphite discs. Microwave plasma CVD is widely used to grow other carbon materials with differences in growth parameters (precursor gas, temperature, pressure, microwave power) leading to different allotropes being formed most notably Carbon-Nanotubes (CNT) [28, 29] and diamond [30, 31]. Initially,  $^{12}\text{C}$  precursor gas, using a system pressure of 1000 Pa with a flow rate of  $50\text{ cm}^3\text{ min}^{-1}$ , was used, primarily due to the high cost of labelled isotopic gases, and with the use of scanning electron microscopy the surface topography was found to be very similar to the 'cauliflower-like' deposits found on irradiated graphite [3]. However, after sectioning with a focused ion beam it was found that the internal morphology was more porous than the deposit found on irradiated graphite. This is believed to be due to the growth rate, approximately  $50\text{ }\mu\text{m hour}^{-1}$ , of the deposit being too rapid to allow a dense deposit to be formed. By comparison, growth rates of diamond using microwave plasma CVD are usually in the region of  $1\text{ }\mu\text{m hour}^{-1}$  [32] and these form 'solid' deposits. By increasing the methane concentration in the precursor gas mix an increased density in the deposit was achieved, likely due to the increased availability of carbon radicals available for deposition. It should be noted that the deposits formed on irradiated graphite are formed at conditions that are very difficult to replicate, pressures of 1-3 MPa, temperatures of approximately  $400\text{ }^\circ\text{C}$  and in the presence of a neutron flux [33], therefore the high density of the deposits found on irradiated graphite is likely due to the high pressure environment, whereas in microwave plasma CVD low pressures are used so that the plasma can be sustained. Further experiments were carried out to investigate the parameters which can affect the growth rate of carbonaceous deposits and to determine whether a more representative carbonaceous deposit could be formed using microwave plasma CVD. Experiments carried out at 200 W using 2, 10 & 20%  $\text{CH}_4$  failed to generate carbonaceous deposits. However, deposition at 400 W induced a rapid growth of carbonaceous material. Further tests were carried out at both 5000 & 10000 Pa pressures using 10%  $\text{CH}_4$ . Deposits were produced for both pressures; however these deposits showed a thin agglomeration of carbonaceous spheres on the graphite substrate. This difference in form and thickness shows that growth at higher pressures is not suitable in producing an analogous material for studying irradiated material. At pressures of 500 Pa with the reduced flow rate the deposit was not analogous of those found in irradiated material, suggesting that the most representative

deposit is formed at system pressure of 1000 Pa with a  $50 \text{ cm}^3 \text{ min}^{-1}$  flow of 10%  $\text{CH}_4$ :90% Ar.

Growth using  $^{13}\text{C}$  precursor gas showed a similar topography/morphology to  $^{12}\text{C}$  deposits indicating that there is no appreciable difference in the growth mechanism between the different isotopes, thereby justifying the use of this simulant to study the behaviour of carbonaceous deposits found on irradiated graphite. The clear separation of the deposit and underlying graphite shown by isotopic imaging using a MS-SIMS has shown that a deposit is formed, and cross-sectional images indicate that the topography and morphology are very similar to the ones found on irradiated graphite. Catalyst stage Raman spectroscopy combined with TGA have shown these deposits to be of a similar reactivity to those found on irradiated graphite. These deposits appear to be suitable for further studies involving microbial systems to examine the possible release of the deposit into the environment in a geological disposal facility. Based on the thermal oxidation behaviour, the density difference in the surface deposit materials between irradiated and simulant samples does not appear to significantly influence observed reactivity. With the surface layers exhibiting rapid degradation at much lower temperatures than the underlying graphite.

## 5. Conclusion

Carbonaceous  $^{12}\text{C}$  and  $^{13}\text{C}$  deposits were formed on Pile Grade A graphite using microwave plasma deposition and examined using Focused Ion Beam, Scanning Electron Microscopy and Magnetic Sector-Secondary Ion Mass Spectrometry. Several conclusions can be drawn:

1. The surface topography of both  $^{12}\text{C}$  and  $^{13}\text{C}$  deposits formed by MPCVD are very similar to the 'cauliflower-like' deposits found on graphite samples trepanned from a Magnox reactor.
2. Deposits formed at 1000 pa system pressure with a  $50 \text{ cm}^3 \text{ min}^{-1}$  flow of 10%  $\text{CH}_4$ :90% Ar showed the closest resemblance to the deposits on the irradiated material.
3. The internal morphology of the deposit is slightly more porous than that found in irradiated graphite. However, variations in methane concentrations and gas pressure can affect the density of deposited material.

To summarise, there is a potential use of the  $^{13}\text{C}$  containing deposits synthesised in this work to act as simulants in future studies aimed at better understanding and predicting the post-

disposal behaviour of irradiated graphite waste in a geological disposal environment and the associated release profile of  $^{14}\text{C}$  arising from the labile deposit.

## Acknowledgements

The authors would like to thank the EPSRC and Radioactive Waste Management for the funding of this work (The post-disposal Behaviour of C-14 and Irradiated Graphite [BIG], Grant No EP/1036354/1). The support of our co-workers at the University of Huddersfield ([www.hud.ac.uk/c-14-big](http://www.hud.ac.uk/c-14-big)) and advice from colleagues in Magnox Ltd and the National Nuclear Laboratory is also gratefully acknowledged.

## References

- [1] Nuclear Decommissioning Authority. Higher Activity Waste, The Long-term Management of Reactor Core Graphite Waste Credible Options (Gate A), SMS/TS/D1-HAW-6/002/A 2013.
- [2] Nuclear Decommissioning Authority. Geological Disposal, Carbon-14 Project – Phase 1 Report, NDA/RWMD/092 2012.
- [3] Heard PJ, Payne L, Wootton MR, Flewitt PEJ. Evaluation of surface deposits on the channel wall of trepanned reactor core graphite samples. *Journal of Nuclear Materials*. 2014;445(1–3):91-7.
- [4] Payne L, Heard, P. J, Scott T. B. Enrichment of C-14 on Surface Deposits of Oldbury Reactor Graphite Investigated with the Use of Magnetic Sector Secondary Ion Mass Spectrometry Waste Management Symposia 2015 Proceedings. 2015.
- [5] Hou X. Rapid analysis of  $^{14}\text{C}$  and  $^3\text{H}$  in graphite and concrete for decommissioning of nuclear reactor. *Applied Radiation and Isotopes*. 2005;62(6):871-82.
- [6] Baston G, Marshall T, Otlet R, Walker A, Mather I, Williams S. Rate and speciation of volatile carbon-14 and tritium releases from irradiated graphite. *Mineralogical Magazine*. 2012;76(8):3293-302.
- [7] Malesevic A, Vizireanu S, Kemps R, Vanhulsel A, Haesendonck CV, Dinescu G. Combined growth of carbon nanotubes and carbon nanowalls by plasma-enhanced chemical vapor deposition. *Carbon*. 2007;45(15):2932-7.
- [8] Bystrov K, Westerhout J, Matveeva M, Litnovsky A, Marot L, Zoethout E, et al. Erosion yields of carbon under various plasma conditions in Pilot-PSI. *Journal of Nuclear Materials*. 2011;415(1):S149-S52.
- [9] Wang SG, Zhang Q, Yoon SF, Ahn J, Yang DJ, Wang Q, et al. Electron field emission from carbon nanotubes and undoped nano-diamond. *Diamond and Related Materials*. 2003;12(1):8-14.
- [10] McConnell ML, Dowling DP, Pope C, Donnelly K, Ryder AG, O'Connor GM. High pressure diamond and diamond-like carbon deposition using a microwave CAP reactor. *Diamond and Related Materials*. 2002;11(3–6):1036-40.
- [11] Castro M, Cuerno R, Nicoli M, Vázquez L, Buijnsters JG. Universality of cauliflower-like fronts: from nanoscale thin films to macroscopic plants. *New Journal of Physics*. 2012;14(10):103039.
- [12] Wickham, AJ, Sellers, RM, Pilkington, NJ. Graphite Core Stability During "Care and Maintenance" and "Safe Storage". Vienna, IAEA-TECDOC 1043. 1998.
- [13] Wickham, AJ, Rahmani, L. Graphite dust explosibility in decommissioning: A demonstration of minimal risk. Vienna, IAEA-TECDOC-1647. 2010.
- [14] Burcl, R. Characterization, Treatment and Conditioning of Radioactive Graphite from Decommissioning of Nuclear Reactors. Vienna, Austria, IAEA-TECDOC-1521. 2006.

- [15] Minshall P, Sadler I, Wickham A. "Radiolytic Graphite Oxidation Revisited". Poster presented at' Specialists meeting on graphite moderator lifecycle behaviour. Bath (United Kingdom): IAEA; 1996.
- [16] Moskovic R, Heard PJ, Flewitt PEJ, Wootton MR. Overview of strength, crack propagation and fracture of nuclear reactor moderator graphite. *Nuclear Engineering and Design*. 2013;263(0):431-42.
- [17] May PW. Diamond thin films: a 21st-century material. *Philosophical Transactions of the Royal Society of London Series A: Mathematical, Physical and Engineering Sciences*. 2000;358(1766):473-95.
- [18] Harton SE, Stevie FA, Ade H. Carbon-13 Labeling for Improved Tracer Depth Profiling of Organic Materials Using Secondary Ion Mass Spectrometry. *J Am Soc Mass Spectrom*. 2006;17(8):1142-5.
- [19] Silbermann G, Moncoffre N, Toulhoat N, Béreard N, Perrat-Mabilon A, Laurent G, et al. Temperature effects on the behavior of carbon 14 in nuclear graphite. *Nuclear Instruments and Methods in Physics Research Section B: Beam Interactions with Materials and Atoms*. 2014;332(0):106-10.
- [20] Lancashire UoC. Contaminated material patent GB1312312.0. 2013 9th July 2013
- [21] Heard PJ, Feeney KA, Allen GC, Shewry PR. Determination of the elemental composition of mature wheat grain using a modified secondary ion mass spectrometer (SIMS). *The Plant Journal*. 2002;30(2):237-45.
- [22] Heard PJ, Wootton MR, Moskovic R, Flewitt PEJ. Crack initiation and propagation in pile grade A (PGA) reactor core graphite under a range of loading conditions. *Journal of Nuclear Materials*. 2010;401(1–3):71-7.
- [23] Lee JS, Gilmore I, Seah M, Fletcher I. Topography and Field Effects in Secondary Ion Mass Spectrometry – Part I: Conducting Samples. *J Am Soc Mass Spectrom*. 2011;22(10):1718-28.
- [24] Kita NT, Ushikubo T, Fu B, Valley JW. High precision SIMS oxygen isotope analysis and the effect of sample topography. *Chemical Geology*. 2009;264(1):43-57.
- [25] Rangarajan S, Tyler BJ. Topography in secondary ion mass spectroscopy images. *Journal of Vacuum Science & Technology A*. 2006;24(5):1730-6.
- [26] Rajsiri S, Kempshall B, Schwarz S, Giannuzzi L. FIB Damage in Silicon: Amorphization or Redeposition? *Microscopy and Microanalysis*. 2002;8(S02):50-1.
- [27] C14-BIG. 2014 [cited; Available from: <http://www.hud.ac.uk/c14-big/>]
- [28] Bower C, Zhou O, Zhu W, Werder DJ, Jin S. Nucleation and growth of carbon nanotubes by microwave plasma chemical vapor deposition. *Applied Physics Letters*. 2000;77(17):2767-9.
- [29] Qin LC, Zhou D, Krauss AR, Gruen DM. Growing carbon nanotubes by microwave plasma-enhanced chemical vapor deposition. *Applied Physics Letters*. 1998;72(26):3437-9.
- [30] Kobashi K, Nishimura K, Kawate Y, Horiuchi T. Synthesis of diamonds by use of microwave plasma chemical-vapor deposition: Morphology and growth of diamond films. *Physical Review B*. 1988;38(6):4067-84.
- [31] Stoner BR, Glass JT. Textured diamond growth on (100)  $\beta$ -SiC via microwave plasma chemical vapor deposition. *Applied Physics Letters*. 1992;60(6):698-700.
- [32] Yan C-s, Vohra YK, Mao H-k, Hemley RJ. Very high growth rate chemical vapor deposition of single-crystal diamond. *Proceedings of the National Academy of Sciences*. 2002;99(20):12523-5.
- [33] Jensen, SE, Nonbol, E Description of the Magnox Type of Gas Cooled Reactor (MAGNOX), NKS/RAK-2(97)TR-C5. 1999.